NATO-SET-312/RSM – Exploiting Radar Data Domains for Classification with Spatially Distributed Nodes

Ronny Gerhard Guendel, Nicolas Christian Kruse, Francesco Fioranelli, Alexander Yarovoy
Microwave Sensing Signals and Systems, Department of Microelectronics, TU Delft, Delft
THE NETHERLANDS

r.guendel@tudelft.nl

ABSTRACT

Recognition of continuous human activities is investigated in unconstrained movement directions using multiple spatially distributed radar nodes, where activities can occur at unfavourable aspect angles or occluded perspectives when using a single node. Furthermore, such networks are favourable not only for the aforementioned aim, but also for larger controlled surveillance areas that may require more than just one sensor. Specifically, a distributed network can show significant differences in signature between the nodes when targets are located at long distances and different aspect angles. Radar data can be represented in various domains, where a widely known domain for Human Activity Recognition (HAR) is the micro-Doppler spectrogram. However, other domains might be more suitable for better classification performance or are superior for low-cost hardware with limited computational resources, such as the Range-Time or the Range-Doppler domain. An open question is how to take advantage of the diversity of information extractable from the aforesaid data domains, as well as from different distributed radar nodes that simultaneously observe a surveillance area. For this, data fusion techniques can be used at both the level of data representations for each radar node, and across the different nodes in the network. The introduced methods of decision fusion, where typically one classifier operates on each node, or feature fusion, where the data is concatenated before using one single classifier, will be exploited, investigating their performance for continuous sequence classification, a more naturalistic and realistic way of classifying human movements, also accounting for inherent imbalances in the dataset.

1.0 INTRODUCTION

Radar networks have demonstrated their advantages in terms of adaptive ability, classification metrics, and tracking performance. This is achieved by increasing the overall information content thanks to multi-perspective views on the scene and targets of interest. Nonetheless, the efficient and effective utilization of radars in a network relies on the aptitude to reliably combine the diverse information from the different sensors. Recently, distributed networks with multiple cooperating radars have attracted significant interest to address issues of micro-Doppler (mD spec.) signatures recorded at unfavourable aspect angles, occlusions, or of targets visible to just a few observer nodes [1]–[10].

In this context, finding the best technique for the fusion of information from multiple radar nodes in a network in order to improve classification performances, remains an outstanding research problem. This is specifically important for the classification of sequences of continuous human activities. These are increasingly investigated in the literature, as opposed to more conventional classification of artificially separated activities recorded in isolation, as they are more realistic and natural [11]–[13].

This paper investigates machine-learning classifiers applied on fused data from a network of nodes with the focus on feature fusion (‘early fusion’) and decision fusion (‘late fusion’) approaches, which are validated on an openly available data set [14]. In this context, the majority of research work has focused mostly on the micro-Doppler (mD) spectrogram as the data format of interest, while this work exploits the following domains additionally, namely the range-Doppler (RD), Fourier synchro-squeezed transform (FSST)

spectrum, and the range-time (RT) map. Information fusion of these data domains is investigated in this paper jointly with radar node fusion across the network. It should be noted that this problem of efficient and effective data fusion across the different data formats and the different radar nodes in the network can be relevant not just to the context of human activity classification, but in any problem of surveillance and situational awareness when information from distributed radar nodes can be used.

In terms of methodology, first the information from each of the aforementioned data domains is extracted by exploiting one-dimensional Principal Component Analysis (PCA) based on Singular Value Decomposition (SVD), a simple yet effective tool to extract features of images for classification. Fioranelli et. al. [3] show for instance the use of SVD-related features to analyse human multistatic walking scenarios with different angular trajectories. It is proposed that SVD can be used to extract the most relevant features from a mD spectrogram by using a limited number of left-sided singular vectors, that are related to the highest singular values. In [3] it is demonstrated that classification results of more than 90% and ideally of 96% for the best angle of the trajectory can be achieved, whilst using very few or even just the single highest related singular value.

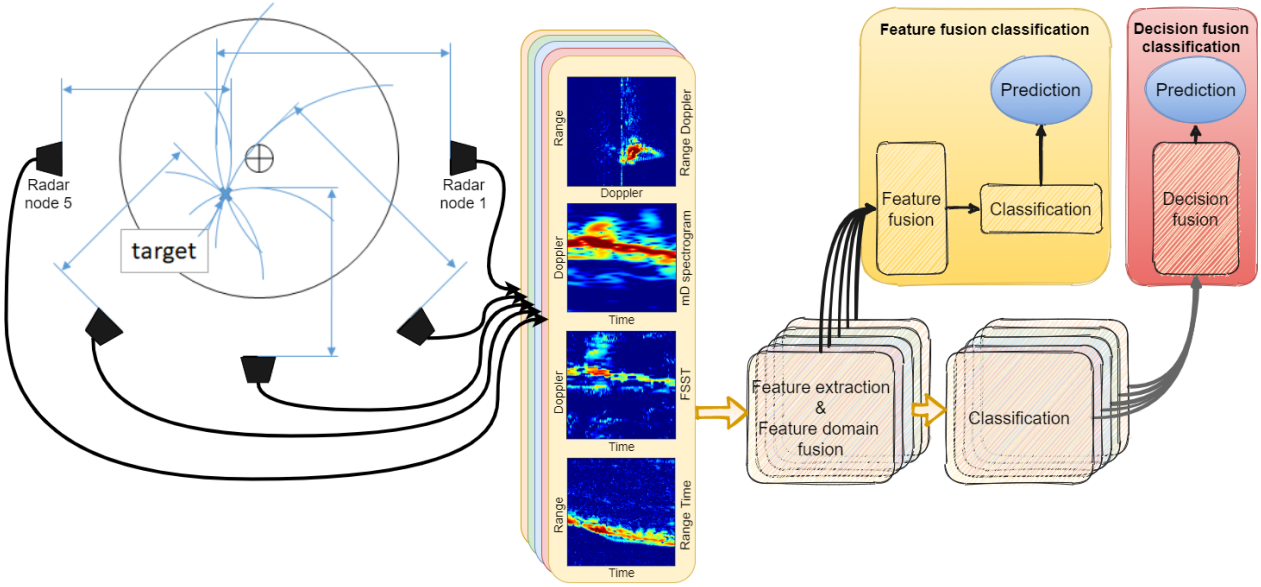

Figure 1: Schematic of the proposed methodology: the extracted data domains from the individual radar nodes are combined ('data domain fusion'). Decision fusion or feature fusion is then applied to combine the information from the nodes.

Then, in this work two-dimensional principal component analysis (2D PCA) based on matrix eigen-decomposition is also investigated, which is shown to result in better accuracy and decreased computation time. For both feature extraction methods four machine learning classifiers, namely the decision tree (DT) classifier, the k-nearest neighbour (KNN) classifier, the naïve Bayes (NB) classifier, and the support vector machine (SVM), are employed to evaluate the aforementioned fusion methods, with a schematic example shown in Figure 1.

The rest of the paper is organized as follows. Section 2.0 shows the data domains including data processing parameters. Feature fusion and machine learning methods are provided in Section 3.0. The experimental results are presented in Section 4.0, and final remarks are given in Section 5.0.

2.0 DATA DOMAINS

Four different data domains are used, as shown in Figure 2, and extracted from each of the five nodes in the network. Specifically, range-Doppler (RD), the mD spectrogram (mD spec.), Fourier synchro-squeezed

transform (FSST) spectrum, and the range-time (RT) map are all extracted. The columns of Figure 2 show examples of the data domains from the 5 different radars, extracted at the same time stamp. The radar system used is a TimeDomain PulsOn radar system P410 with an ultra-wideband UWB chipset, operating at a centre frequency of 4.3 GHz and a bandwidth of about 2.2 GHz. The setup allows a range coverage of 4.38m, and a pulse repetition frequency of 122Hz which results in a unambiguous Doppler velocity of roughly 2.2 m/s [15], [16]. For more information about the recordings and the topology of the 5 distributed radar nodes in the network, references [17], [18] apply.

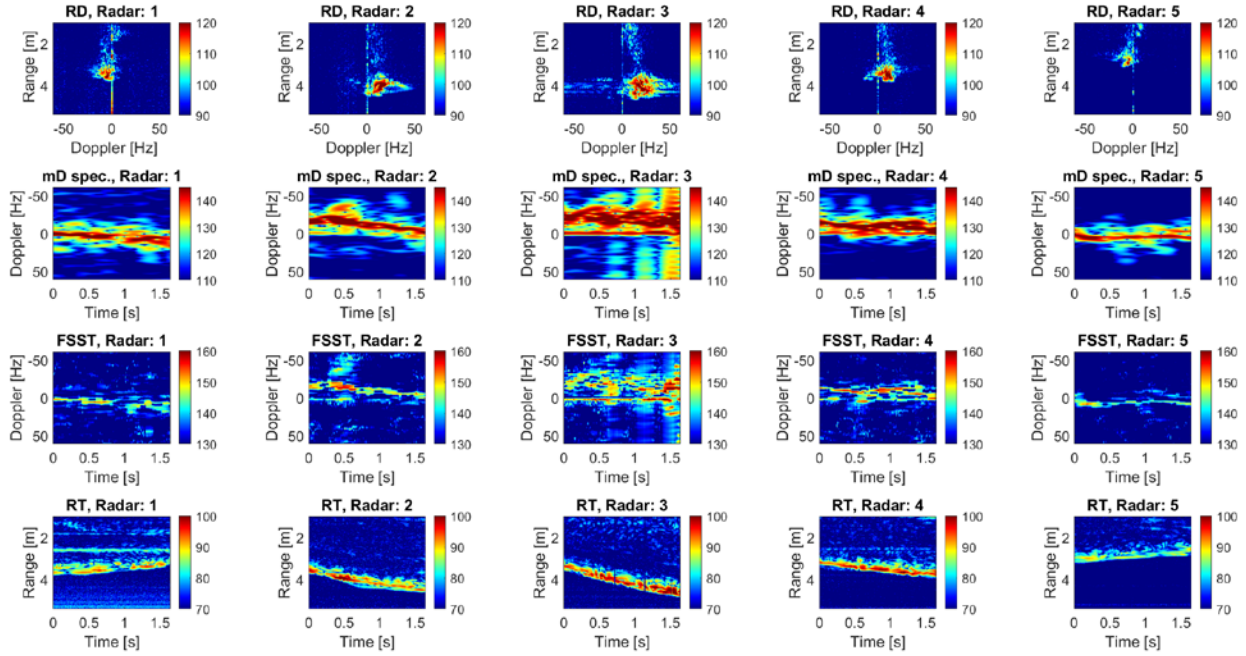

Figure 2: Examples of the 4 radar data domains of namely, range-Doppler (RD), the mD spectrogram (mD spec.), Fourier synchro-squeezed transform (FSST) spectrum, and the range-time (RT) map. For the latter three domains a sliding window of 200 samples (1.64s) was used. The RD processing is instead a FFT computed across the RT with the same 200 samples (1.64s).

The following parameters are applied for further computation of the data domains:

- STFT window (mD spec.): 64 samples (524ms)
- Sliding window[1] and RD parameter:
  - Window size: 200 samples (1.64sec)
  - Hop size: 25 samples (205ms)
- Image size for classification: 224 x 224 pixel

The extracted domain images after resizing are forwarded for feature extraction, as explained in Section 3.0.

3.0 FEATURE EXTRACTION AND MACHINE LEARNING

3.1 Feature extraction using one-dimensional (1D) Principal Component Analysis (PCA)

[1] Sliding window parameters apply to the mD spectrogram, the FSST, and the RT, respectively.

The Principal Component Analysis (PCA) based on Singular Value Decomposition (SVD) is utilised for four HAR typical radar domains, the range-Doppler (RD), micro-Doppler spectrogram (mD spec.), the Fourier synchro-squeezed transform (FSST) spectrum, and the range time (RT) to extract the features, suppress background noise, and reduce data space dimensionality at the same time [19].

In this work, PCA is applied on the down-sampled image domains, such as the ones shown in Figure 2, using a sliding window for mD spec., the FSST, and RT domain of 1.64s. For the RD domain, a window of the same duration is used for computation. The images of each domain are represented by the matrix, X, such that the SVD can be written as

$$X=U\Sigma V^T \qquad (1)$$

with U and V indicating the left and the right singular matrices respectively, consisting of the left and right linearly independent singular vectors u_i and v_i. Note that the image matrix, X, is generally full ranked. Thus, all u_i and v_i vectors are independent.

The matrix Σ contains the singular values $\sigma_i = \Sigma_{ii}$ on the diagonal, where *i* is the number of elements in Σ, and is equivalent to the image size of X. The diagonal entries σ_i are uniquely determined by X. The singular values are commonly used to determine a suitable number of left-sided singular vectors that are able to provide appropriate noise suppression and still contain the relevant features. A common practice is determining the "knee" or the "elbow" of the singular values, $\sigma = [\sigma_1, ..., \sigma_k]$, as shown in Figure 3, to truncate the matrices $U \in \Re^{i \times i}$, as $\overline{U} \in \Re^{i \times k}$. $\overline{U}$ represents a new truncated left-sided singular matrix with k indicating the amount of vectors associated with the subset of strongest singular values. In this work, 5 singular values are considered ($k = 5$). The vectors of the left-sided singular value matrix, $\overline{U} = [u_1, u_1, ..., u_k]$, also called principal component vectors, are vertically concatenated to form the feature vector used for classification: $s = [u_1^T, ..., u_k^T]^T$. The formed vector s is the feature vector of one data domain and one radar node. In the case of feature fusion across the nodes in the network, the feature vectors from four ($d = 4$) introduced data domains and up to five radar nodes ($n \leq 5$) are concatenated, as $S = [s_{d=1,n=1}^T, \ldots, s_{d=4,n=1}^T, \cdots, s_{d=1,n=5}^T, \ldots, s_{d=4,n=5}^T]^T$, and forwarded to the classifiers [20].

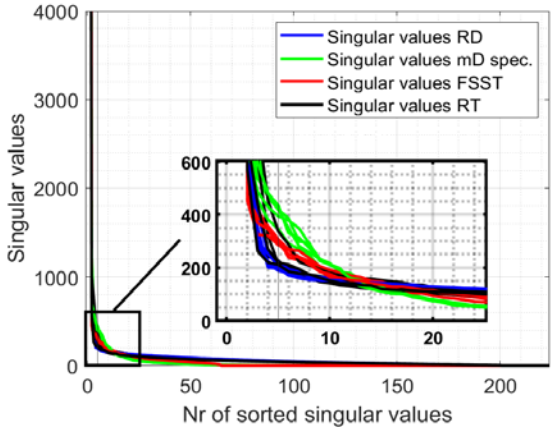

Figure 3: Singular values of the 4 data domains used for range-Doppler (RD), micro-Doppler spectrogram (mD spec.), FSST spectrum and the range-time (RT). A number of $k = 5$ singular values were selected to capture the features of interest and generate the truncate left-sided singular component vectors forming the principal matrix, $\overline{U} \in \Re^{i \times k}$.

3.2 Feature extraction using two-dimensional (2D) Principal Component Analysis (PCA)

In addition to one-dimensional Principal Component Analysis, two-dimensional (2D) Principal Component Analysis (PCA) is also employed to extract the features of the domains RD, mD spec., FSST spec., and RT. To construct the final feature vectors v of each domain, the total covariance matrix, H, is computed for each data domain and each radar as

$$H = \frac{1}{M} \sum_{m=1}^{M} (X^{(m)} - \overline{X})^T \cdot (X^{(m)} - \overline{X})$$

$$HQ = Q\Lambda \qquad (2)$$

$$H = Q\Lambda Q^{-1}$$

m indicates the image sample in the set M, with $\overline{X} \in \Re^{i \times i}$ the mean image $\overline{X} = \frac{1}{M} \sum_{m=1}^{M} X^{(m)}$. Eigen-decomposition on the covariance matrix H is applied to compute the eigenvector matrix Q, and eigenvalue matrix Λ, the latter containing the eigenvalues λ. The *k* strongest eigenvalues $[\lambda_1, ..., \lambda_k]$ are identified by finding the "knee" or "elbow" to determine the number of sufficient eigenvectors such as $\overline{Q} = [q_1, q_2, \ldots, q_k]$ forming $\overline{Q} \in \Re^{i \times k}$. The set of feature vectors is obtained by projecting each image $X^{(m)}$ on the matrix of truncated eigenvectors $\overline{Q}$, as $\overline{Y} = X\overline{Q}$, such that $\overline{Y}$ equals the matrix of projected feature vectors and is of dimension, $\overline{Y} \in \Re^{i \times k}$. The vectors constituting matrix $\overline{Y}$ are called the principal component vectors of the sample image $X^{(m)}$. Finally, the principal component vectors are concatenated to obtain the feature vector $v \in \Re^{ik \times 1}$. As for 1D PCA, the feature vectors of all domains ($d = 4$) and up to

five radar nodes ($n \leq 5$) are concatenated, as $S = [s^T_{d=1,n=1}, \ldots, s^T_{d=4,n=1}, \cdots, s^T_{d=1,n=5}, \ldots, s^T_{d=4,n=5}]^T$, and forwarded to the classifiers [21].

3.3. Classification and fusion

Data fusion is investigated in this paper using feature fusion ('early fusion') and decision fusion ('late fusion'), as the flow graph in Figure 4 shows. Let the data domain be the image matrix, $X \in \Re^{i \times i}$. The extracted feature vectors are of dimension $v \in \Re^{ik \times 1}$, with k the selected principal components. The introduced 4 domains, d, are RD, mD spec., FSST spec., and RT, increasing the feature vector length to $v_{all} \in \Re^{ikd \times 1}$ per radar node. Then, decision fusion can be applied on each node using the feature vector s_{all} of size $ikd \times 1$. This classification approach might be even suitable for decentralized systems, where an initial classification is performed locally at each node, and only the decisions and related confidence levels are passed and shared among different nodes.

It will be assumed that the classifier predicts the probability of each class as $\hat{p}_{cl}$, according to the information of the feature vector s_{all} and the training procedure. In principle, the last layer of a classifier determines predicted class by calculating the highest probability as $\hat{y} = \underset{cl}{argmax}\left[\hat{p}_{cl}\right]$, with $\hat{y}$ the predicted class and cl the classes. Beforehand, decision fusion can combine the prediction probabilities of each node n to have an overall decision from the radar network, as:

$$\hat{P}^{(m)}_{cl} = Mean\left(\hat{p}^{(m)}_{cl}\right) = \frac{1}{N}\sum_{n=1}^{N} \hat{p}^{(m)}_{cl,n} \qquad (3)$$

where N indicates the set of the radar nodes and m the sample index. The predicted class is computed as $\hat{y} = \underset{cl}{argmax}\left[\hat{P}_{cl}\right]$. The sample superscript $(\square)^{(m)}$ will be neglected for better readability.

For decision fusion, the feature vector grows by the number ($n \leq 5$) of radars in the network, $V \in \Re^{ikdn \times 1}$. While the prediction of classes follows the same approach as for feature fusion, the combination of probability vectors, as shown in Eq (3) is not needed here, since only one classifier is used for classification, as shown in Figure 4.

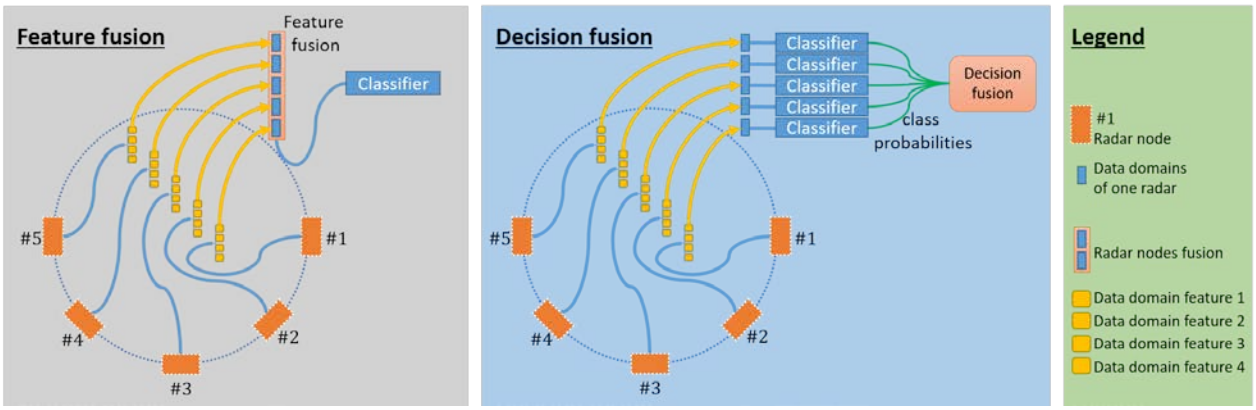

Figure 4: Flow graph with pipeline using feature fusion and decision fusion of the 5 radar nodes and 4 data domains considered in this paper.

However, it should be noted that the prediction vector for each sample has the size of the total number of classes, instead of $ikd \times 1$ for decision fusion or even $ikdn \times 1$ for feature fusion. It can be expressed as $length(V) \square\ length(v_{all}) \square\ length(\hat{P}_{cl}) = length(\hat{p}_{cl})$. It is important to note that forwarding the feature vectors v_{all} of each radar to a centralized system to form V can become computationally heavy and demanding in terms of communication bandwidth, especially if there are a lot of features to be considered. A proposed solution is the usage of decision fusion, which requires only the transmission of probability vector $\hat{p}_{cl}$ between the nodes. The trade-off is that feature fusion provides, on average, a higher classification accuracy [18] and can give more degrees of freedom in selecting different features from different nodes ('feature diversity').

4.0 RESULTS

Initial results are generated for feature fusion ('early fusion') and for decision fusion ('late fusion') across the used radars and data domains. These classification results are presented with the following input domains: range-Doppler (RD), micro-Doppler spectrogram (mD spec.), Fourier synchro-squeezed transform spectrum (FSST), and the range-time map (RT). Example images of sliding window instances of these domains are provided in Figure 2.

The evaluated classifiers in this work are:

- the decision tree (DT) classifier
- the k-nearest neighbour (KNN) classifier {five neighbours, Euclidean distance}
- the naïve Bayes (NB) classifier
- the support vector machine (SVM) {Gaussian kernel}

Results are provided for the training accuracy, the validation accuracy when using an hold-out of 30% of the training data, and the leave one person out (L1Po) test for each individual participant of the training data.

The first section focuses on feature fusion (early fusion) and decision fusion (late fusion) using 1D Principal Component Analysis (1D PCA), and the subsequent section covers 2D PCA in a similar fashion.

4.1 Using one-dimensional (1D) Principal component analysis

This section contains the results for the application of feature fusion and decision fusion across the radar nodes and the data domains, after extracting features using 1D PCA. PCA is applied to the images that are extracted from a window of 200 samples (1.64s), as illustrated in Figure 1, with a down-sampled image size of 224×224 pixels and followed by singular value decomposition (SVD). The left-sided singular vectors are indicated as $\overline{U} \in \Re^{224 \times k}$, where *k* is the number of left-sided singular vectors associated with the highest singular values $[\sigma_1, ..., \sigma_k]$. The singular vectors are vertically concatenated to obtain the feature vector $s \in \Re^{224 \cdot k \times 1}$. Feature fusion over domains and radar nodes is accomplished by concatenating the feature vectors s for all five available nodes and for all four domains, resulting in a total feature vector $S \in \Re^{224 \cdot k \cdot d \cdot n \times 1}$, with *d* and *n* indicating the amount of domains and nodes respectively. In this work, $k = 5$, $d = 4$, and $n \leq 5$, resulting in a maximum total feature vector of length $224 \cdot 4 \cdot 4 \cdot 5 = 22400$.

The results are displayed in Table 1 and in Figure 5, where the top grey part of Table 1 shows the accuracy, and the yellow bottom shows the average F1 score across all classes. In the table and figure, the performance for the various classifiers under evaluation is presented for varying combinations of radar nodes, and for all three evaluation approaches: Test, cross-validation, and L1Po.

First, the full set of nodes is considered, indicated as R: 1,2,3,4,5. Here, the NB classifier performs worst in the training stage, whereas it achieves the highest L1Po results with an average F1 score of 46.4%, and the second-highest total accuracy (61.2%) after the KNN classifier (64.0%). Inspection of relevant confusion matrices reveals that the KNN classifier suffers from minority class classification, which is reflected in the difference between the accuracy and the F1 score.

By decreasing the amount of utilised radar nodes, a performance degradation is expected. This degradation is demonstrated in the R:3 rows of the table, where a decrease of (46.4% → 34.8%) for the L1PO NB average F1 score and of (61.2% → 39.9%) in accuracy can be seen. Likewise, the decrease is also present for the other classifiers, though to a lesser extent. In general, the L1Po performance of SVM is inferior to the other tested classifiers. This is possibly attributable to an overfitting problem of the SVM classifier due to the unfavourable training data vs. feature vector length ratio, i.e. the relatively long feature vector with respect to the size of the available data samples [22], [23].

Table 1: Feature fusion accuracy and F1 score results using from one radar (radar node 3, indicated as, R: 3) up to all radars in the network, indicated as R: 1,2,3,4,5. The features are extracted with 1D PCA using 5 singular vectors from four domains: Range-Doppler (RD), micro-Doppler spectrogram (mD spec.), Fourier synchro-squeezed transform spectrum (FSST), and the range-time map (RT). They are subsequently concatenated and forwarded to the classifiers. The tested classifiers are the decision tree (DT), k-nearest neighbour (KNN), Naïve Bayes (NB), and support vector machine (SVM).

Accuracy	Training				Cross validation 70/30				L1Po test			
Radar nodes	DT	KNN	NB	SVM	DT	KNN	NB	SVM	DT	KNN	NB	SVM
R: 3	92.8	76.7	47.3	70.6	57.4	65.2	43.7	45.1	48.3	58.9	39.9	44.2
R: 1,5	93.4	77.2	53.9	88.8	56.4	65.4	49.8	40.8	52.8	59.5	46.5	40.5
R: 2,4	93.2	79.3	61.6	89.3	59.1	67.2	59.1	44.3	51.1	60.9	55.6	39.1
R: 1,3,5	93.2	78.6	59.1	97.5	57.8	67.8	55.4	41.1	53.8	61.1	51.4	41.0
R: 1,2,3,4,5	93.6	81.4	68.4	100.0	59.5	71.2	64.0	47.1	53.5	**64.0**	61.2	41.8
F1 score	**Training**				**Cross validation 70/30**				**L1Po test**			
Radar nodes	**DT**	**KNN**	**NB**	**SVM**	**DT**	**KNN**	**NB**	**SVM**	**DT**	**KNN**	**NB**	**SVM**
R: 3	86.9	62.6	42.5	62.1	41.2	45.6	38.5	26.8	31.6	33.2	34.8	23.2

R: 1,5	88.1	64.1	49.2	88.5	40.2	43.5	44.1	26.0	33.1	29.5	35.7	25.0
R: 2,4	88.1	67.2	54.3	89.2	42.6	47.4	50.0	29.7	32.3	35.6	42.2	22.6
R: 1,3,5	87.5	66.6	53.2	97.6	40.3	48.1	48.1	28.0	33.4	33.5	39.2	24.1
R: 1,2,3,4,5	88.6	69.0	61.4	100.0	43.5	50.8	54.7	32.6	34.2	33.0	**46.4**	26.1

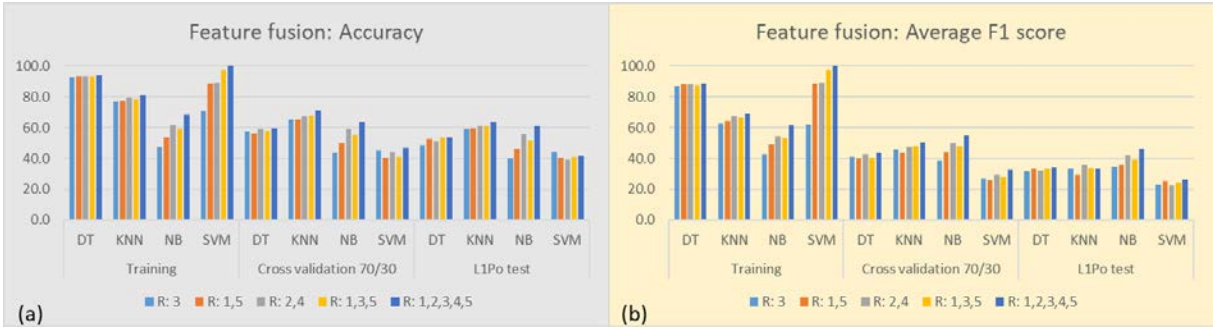

Figure 5: Results using 1D Principal component analysis (1D PCA) with 5 singular vectors by applying early fusion (feature fusion) across all data domains and radar nodes. R: XX stands for the selected radar nodes, e.g., R: 3 indicates node 3; all nodes are indicated as R: 1,2,3,4,5. (a) shows the achieved accuracy and, (b) the average F1 score across all five classes, respectively.

Table 2 and Figure 6 provide the classification results for the individual data domains of RD, mD spec. FSST, and RT using the full set of 5 radars in the network. The NB classifier with L1Po validation attains the best F1 score with 44.9% using the mD spec. domain, followed by the FSST domain with 42.1%. The highest L1Po accuracy is achieved by the KNN classifier with 57.1% using the RD domain and followed by the RT domain with 56.9%. From the F1 scores of the L1Po results, all data domains are suitable to use, with the overall best performance reached by the NB classifier. The SVM classifier may suffer again from overfitting as described earlier.

Table 2: The accuracy and F1 score results of the individual data domains, RD, mD spec. FSST, and RT using the full set of 5 radars in the network. The features from each domain and radar are extracted using 1D PCA. Hence, the same features from each radar are vectorized and concatenated for the classifiers of DT, KNN, NB, and SVM.

Accuracy	**Training**				**Cross validation 70/30**				**L1Po test**			
Datadomain	**DT**	**KNN**	**NB**	**SVM**	**DT**	**KNN**	**NB**	**SVM**	**DT**	**KNN**	**NB**	**SVM**
Range Doppler	93.5	77.9	54.8	88.1	60.4	65.2	51.0	37.3	50.4	**57.1**	48.6	35.9
mD spec.	91.2	75.3	56.8	69.3	58.8	57.1	55.1	48.2	53.9	53.6	53.7	48.3
FSST	93.2	73.8	58.8	69.2	58.3	58.6	55.8	47.7	52.9	54.0	54.6	49.8
Range Time	93.0	78.9	54.4	89.9	55.2	68.0	51.7	45.8	44.2	56.9	45.5	42.6
F1 score	**Training**				**Cross validation 70/30**				**L1Po test**			
Datadomain	**DT**	**KNN**	**NB**	**SVM**	**DT**	**KNN**	**NB**	**SVM**	**DT**	**KNN**	**NB**	**SVM**
Range Doppler	88.4	64.9	49.8	88.6	44.3	45.1	43.3	24.5	30.5	30.7	35.5	20.7
mD spec.	86.6	58.5	51.9	59.1	42.4	38.0	45.1	29.6	30.4	31.1	**44.9**	29.4
FSST	87.4	59.0	50.4	59.6	41.7	39.0	44.8	28.2	33.1	31.0	42.1	28.3
Range Time	87.7	68.6	48.7	89.0	41.6	51.8	43.3	29.9	29.0	34.0	31.9	23.1

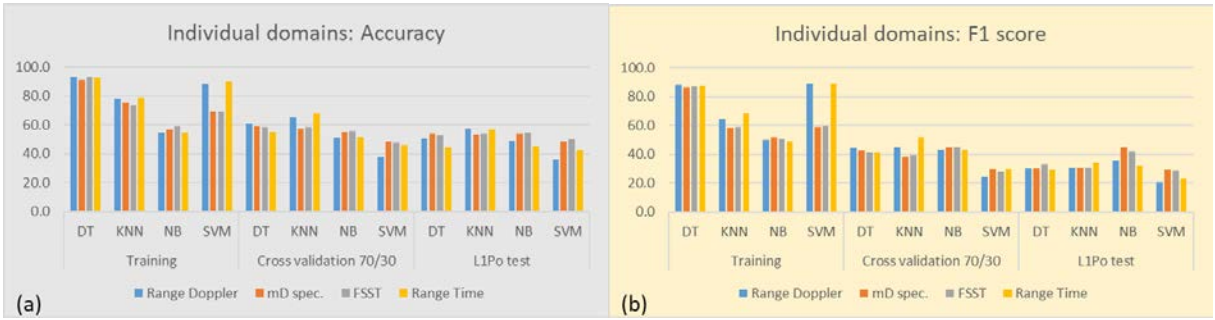

Figure 6: Results for individual data domain classification of RD, mD spec., FSST, and RT, using 1D PCA (5 singular vectors) to extract the features and fuse the individual domains by applying early fusion (feature fusion) for the five radar nodes only (hence, not across data domains).

Figure 7 shows the results for late fusion (i.e., decision fusion) across the class probability outputs of each classifier. Here, the full set of radars is used. Again, NB with a L1Po F1 score of 35.5% performs best, while the best L1Po accuracy is achieved by the KNN classifier with 57.1%, with the results seen in Figure 7. The KNN classifier again performs best for the majority classes of (1) *Walking*, and (2) *Stationary condition*, whereas it suffers for the minority classes of (3) *In-place activities*, (4) *Standing up from the ground*, and (5) *Falling down*. This explains the discrepancy between the relatively high accuracy and the comparatively low F1 scores for the KNN classifier in the specific imbalanced dataset used in this study.

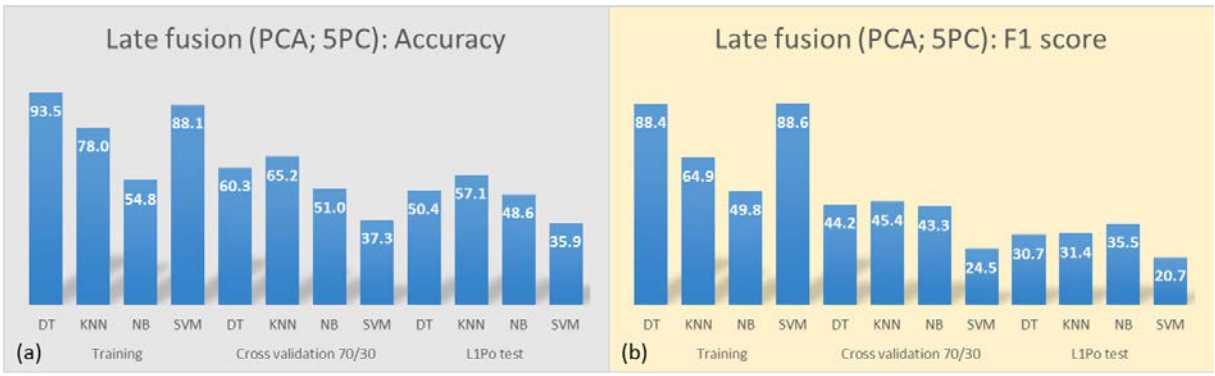

Figure 7: Results for 1D PCA with 5 singular vectors by applying late fusion (decision fusion) across the class probabilities of the individual data domains for the full set of 5 radars.

In summary, this section shows the results for feature fusion, individual data domain classification, as well as decision fusion across the individual domains. Feature extraction is accomplished by means of 1D PCA of the four domains, a common feature extraction method, utilizing only the left-sided singular vectors. The overall best performance is attained when evaluating the L1Po performance by using feature fusion applied on all domains and radar nodes. Specifically, the KNN classifier reached an accuracy of 64%, and the NB classifier achieves a 44.9% F1 score.

4.2 Using two-dimensional (2D) Principal component analysis

As in the previous section, results for using feature fusion and decision fusion across the radar nodes and the data domains are presented here. Feature extraction is this section is accomplished using two-dimensional principal component analysis (2D PCA) based on matrix eigen-decomposition. As before, 2D PCA is applied to the images, as illustrated in Figure 2, with a down-sampled image size of 224×224 pixels. The

feature matrix, $\overline{Y} \in \Re^{224 \times k}$, is extracted from the total covariance matrix, H, where k is the number of selected principal component vectors, associated with the highest eigenvalues $[\lambda_1, ..., \lambda_k]$ after eigenvalue decomposition. The eigenvectors are vertically concatenated to obtain the feature vector $s \in \Re^{224 \cdot k \times 1}$. Feature fusion over data domains and radar nodes is accomplished by concatenating feature vectors *v* for all five available nodes and for all four domains, resulting in a total feature vector $S \in \Re^{224 \cdot k \cdot d \cdot n \times 1}$, with *d* and *n* indicating the amount of domains and nodes respectively. In this work, $k = 5$, $d = 4$, and $n \leq 5$, resulting in a maximum total feature vector of length $224 \cdot 4 \cdot 4 \cdot 5 = 22400$ [24].

The results discussed here are presented in Table 3 and Figure 8, where the top grey part of the Table 3 displays the accuracy, and the yellow bottom shows the average F1 score across all classes. In the table and figure, the performance for the various classifiers under evaluation is presented for varying combinations of radar nodes, and for all three validation approaches.

The best L1Po performance is achieved through the utilization of the full set of 5 nodes, indicated as R: 1,2,3,4,5, by the NB classifier with a 48.3% F1 score. It can be seen that the NB classifier provides the best L1Po accuracy for all node subsets, with the exception of the single R:3 subset. The maximum achieved accuracy is 62.3%, for the R: 1,3,5 subset.

As in the previous section, a performance degradation is expected by decreasing the amount of radar nodes. As an example, the F1 score results for the NB classifier degrades from 48.3% to 22.9% in the L1Po test. The comparatively poor L1Po performance of the SVM classifier seems to suggest that the SVM classifier over-fits in this scenario, and that the feature vectors are too large in relation to the number of samples available in the dataset [22], [23].

Table 3: 2D PCA feature fusion accuracy and F1 score results using from one radar (radar node 3, indicated as, R: 3) up to all 5 radars in the network indicated as, R: 1,2,3,4,5. The features are extracted using 2D PCA with 5 principal component vectors from four data domains, namely, range-Doppler (RD), micro-Doppler spectrogram (mD spec.), Fourier synchro-squeezed transform spectrum (FSST), and the range-time map (RT). The tested classifiers are the decision tree (DT), k-nearest neighbor (KNN), Naïve Bayes (NB), and support vector machine (SVM).

Accuracy	Training				Cross validation 70/30				L1Po test			
Radar nodes	DT	KNN	NB	SVM	DT	KNN	NB	SVM	DT	KNN	NB	SVM
R: 3	95.2	93.2	57.8	100.0	70.4	85.9	56.6	85.2	30.9	25.6	24.3	23.0
R: 1,5	96.7	94.2	68.6	100.0	75.1	86.3	66.2	88.5	53.2	60.6	60.8	29.3
R: 2,4	96.3	94.6	67.1	100.0	77.4	89.2	66.5	90.0	24.1	28.8	39.0	33.2
R: 1,3,5	96.8	95.1	71.2	100.0	76.1	89.8	69.9	90.6	39.9	43.2	**62.3**	19.8
R: 1,2,3,4,5	96.9	94.9	72.2	100.0	80.4	89.5	71.3	92.7	37.4	29.5	60.4	34.2
F1 score	**Training**				**Cross validation 70/30**				**L1Po test**			
Radar nodes	**DT**	**KNN**	**NB**	**SVM**	**DT**	**KNN**	**NB**	**SVM**	**DT**	**KNN**	**NB**	**SVM**
R: 3	91.4	90.5	48.8	100.0	58.0	79.1	47.8	80.4	21.5	16.3	22.9	16.0
R: 1,5	94.5	92.2	56.8	100.0	64.0	81.3	55.0	86.0	33.3	39.5	40.6	22.5
R: 2,4	94.1	92.9	56.7	100.0	67.7	85.5	56.2	87.7	17.3	21.8	35.2	20.1
R: 1,3,5	94.6	93.5	60.8	100.0	66.1	86.0	59.2	88.1	29.9	28.9	47.7	15.5
R: 1,2,3,4,5	94.7	93.3	62.3	100.0	70.9	85.5	60.5	90.5	24.3	21.7	**48.3**	20.8

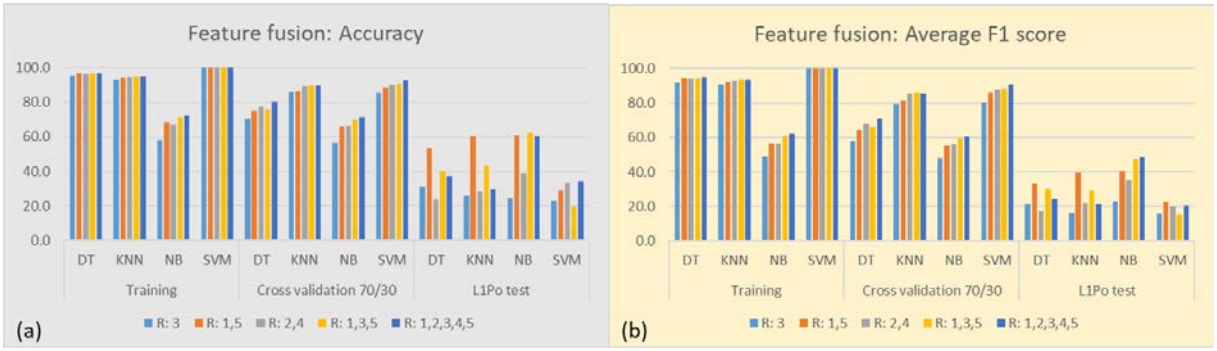

Figure 8: Results using two-dimensional (2D) PCA with 5 principal vectors by applying early fusion (feature fusion) across all domains and radar nodes. R: XX stands for the selected radar nodes, e.g., R: 3 indicates node 3; all nodes are indicated as R: 1,2,3,4,5. (a) shows the achieved accuracy and, (b) the average F1 score across all five classes, respectively.

The classification matrices for the NB classifier are provided in Figure 9. Feature fusion is applied over all 5 nodes and over all data domains. Inspection of these matrices reveals a strong imbalance between the majority classes (1) *Walking* and (2) *Stationary*, and the minority classes such as (5) *falling*. This imbalance can be considered natural for HAR problems, since a fall event firstly happens relatively infrequently, and secondly has generally a shorter duration than extended activities, such as walking. Nonetheless, instances of the walking class have been also wrongly classified as falling, which is unsurprising as the falling class in this dataset also includes falling from a walking motion. Thus, the transition between the classes is a smooth merging of one motion into the other, making it more difficult to classify activities based on fixed-length portions of data.

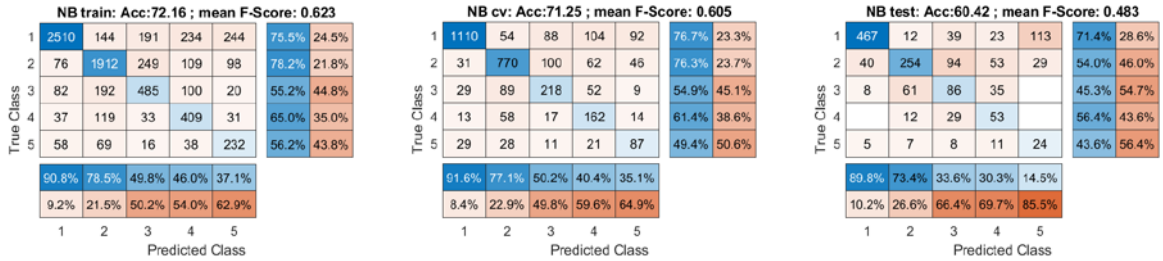

Figure 9: The classification matrices using two-dimensional (2D) PCA with 5 principal vectors by applying early fusion (feature fusion) across all domains and 5 radar nodes are provided. The left matrix shows the achieved training results, the middle matrix the cross-validation results, and the right matrix the L1Po test results, respectively. The classes are: (1) Walking, (2) Stationary condition, (3) In-place activities, (4) Standing up from the ground, (5) Falling down.

Feature fusion of five radars (See Table 1: R: 1,2,3,4,5) using 2D PCA with five and ten eigenvectors (indicated as 5 EV and 10 EV) is evaluated for different data domains, with results shown in Table 4 and Figure 10. The eigenvectors, also called principal components (PC), are those associated with the 10 highest eigenvalues. Looking at the F1 score in the L1Po test, the NB classifier again performs best with 48.2% using the FSST domain and features extracted from 10 PC. However, it should be noted that an increase from 5 to 10 PC enlarges the feature vector by a factor of two, which increases data load and computational complexity.

Additionally, it is apparent that increasing the amount of PC from 5 to 10 for the mD spectrogram and FSST domain grants improvements in the order of 10% and 20%, respectively, whereas this increase results in

negligible changes for the RT and RD domain.

Table 4: The accuracy and F1 score results using two-dimensional (2D) PCA feature extraction of the individual data domains, namely, RD, mD spec., FSST, and RT by using the full set of 5 radars in the network. The tested classifiers are DT, KNN, NB, and SVM for five and ten principal component vectors, indicated as 5PC and 10 PC in the table.

Accuracy	Training				Cross validation 70/30				L1Po test			
Datadomain	**DT**	**KNN**	**NB**	**SVM**	**DT**	**KNN**	**NB**	**SVM**	**DT**	**KNN**	**NB**	**SVM**
Range Doppler; 5 EV	95.6	95.0	71.9	100.0	72.4	89.1	71.1	93.0	45.6	58.7	58.0	51.3
Range Doppler; 10 EV	95.7	95.7	72.2	100.0	72.5	89.9	72.1	94.1	51.5	56.3	**59.3**	53.7
mD spec.; 5 EV	95.4	93.5	68.3	100.0	72.4	87.0	68.0	78.9	23.4	28.8	39.2	20.4
mD spec.; 10 EV	96.0	94.1	69.8	100.0	73.0	87.4	68.2	66.4	25.2	29.0	49.6	20.2
FSST; 5 EV	95.2	92.6	66.9	98.5	71.2	85.0	67.0	71.7	35.9	37.5	38.4	28.6
FSST; 10 EV	95.2	92.7	69.0	100.0	71.2	85.0	67.6	62.3	43.8	32.3	59.2	32.0
Range Time; 5 EV	96.2	94.0	66.3	100.0	78.2	87.7	65.4	84.9	40.0	44.4	58.4	44.1
Range Time; 10 EV	95.9	93.7	65.3	100.0	74.7	87.1	64.4	73.9	48.3	45.9	58.0	43.8
F1 score	**Training**				**Cross validation 70/30**				**L1Po test**			
Datadomain	**DT**	**KNN**	**NB**	**SVM**	**DT**	**KNN**	**NB**	**SVM**	**DT**	**KNN**	**NB**	**SVM**
Range Doppler; 5 EV	92.3	93.4	60.3	100.0	60.7	86.0	58.4	91.6	31.0	39.7	42.6	34.3
Range Doppler; 10 EV	93.0	94.8	62.3	100.0	59.9	86.3	59.2	93.0	32.6	38.9	43.2	36.5
mD spec.; 5 EV	91.9	90.7	58.1	100.0	60.9	81.0	57.5	71.2	15.5	22.3	31.0	14.4
mD spec.; 10 EV	93.2	92.5	60.9	100.0	60.1	81.5	56.2	49.7	19.5	24.2	41.0	14.3
FSST; 5 EV	91.2	89.5	55.5	98.4	58.8	78.0	55.9	60.9	23.2	25.7	28.7	17.0
FSST; 10 EV	92.4	90.3	58.4	100.0	59.0	78.3	54.5	46.3	28.4	23.6	**48.2**	19.6
Range Time; 5 EV	93.6	91.6	54.2	100.0	70.0	83.2	52.3	82.0	28.4	32.7	42.3	33.1
Range Time; 10 EV	93.4	91.9	53.5	100.0	64.3	81.5	50.1	67.1	32.6	32.4	41.3	32.1

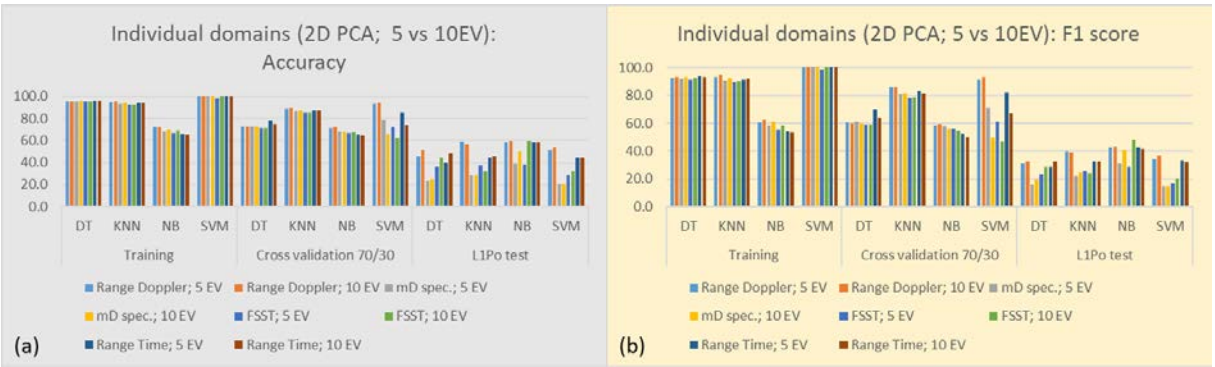

Figure 10: Results using the individual data domain classification of RD, mD spec., FSST, and RT, with 2D PCA with five and ten eigenvalues (5 EV and 10 EV in the figure) to extract the features. The individual data domains of the network are fused by applying early fusion (feature fusion) for the five radar nodes only (not across domains). (a) shows the achieved accuracy and, (b) the average F1 score across all five classes, respectively.

Figure 11 shows the accuracy and average F1 score results using late fusion for the four classifiers. The evaluation strategy again consists of training, cross validation, and L1Po. The best L1Po evaluation is again achieved by the NB classifier (F1 score: 42.6%, accuracy: 58%), followed by the KNN classifier (F1 score: 40.2%, accuracy: 58%), both evaluated across the four domains of RD, mD spec., FSST and RT. The test is conducted with the first five principal vectors, indicated as 5EV.

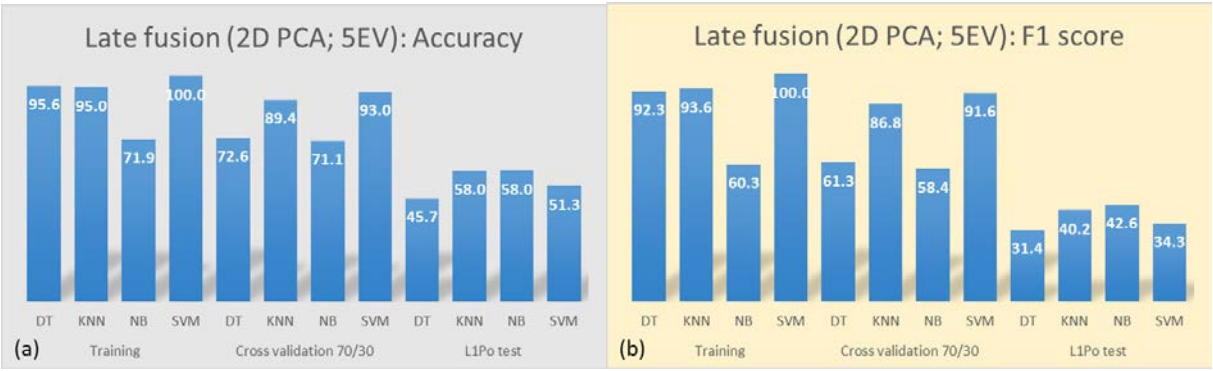

Figure 11: Results using 2D PCA with 5 eigenvectors by applying late fusion (decision fusion) across the class probabilities of the individual domains for the full set of radars. (a) shows the achieved accuracy and, (b) the average F1 score across all five classes, respectively.

5.0 CONCLUSIONS AND FUTURE WORK

This paper investigates radar network sensor fusion architectures using outputs from four selected data domains, the range-Doppler, the micro-Doppler spectrogram, the FSST spectrum, and the range-time map. The considered application is human activity classification. However, the problem of finding the best fusion methods for the possible radar data representation jointly with the number of nodes in the radar network remains open.

In this paper, the best results among all methods are achieved by performing 2D PCA feature extraction and applying feature fusion (‘early fusion’) across all data domains and all 5 radar nodes, yielding 48.3% F1 score using the naïve Bayes (NB) classifier. Furthermore, 2D PCA is shown to have the advantage of a fast total covariance matrix computation, compared to SVD performed for each sample image in the case of 1D PCA. Despite the computational differences, 1D PCA results are comparable, with an average F1 score of 46.4%. The best results using decision fusion (‘late fusion’) are achieved by using 2D PCA and the NB classifier, with an F1 score of 42.6%. It is important to highlight the challenging nature of the data in this dataset, namely that the sequences of human activities are collected in a continuous manner and along unconstrained trajectories. This can explain the lower classification results with respect to other studies in the literature in the same context. Additionally, the classifiers employed in this paper are chosen for their relative simplicity, rather than resorting to state of the art neural networks that are expected to yield the highest performance. This choice is motivated by the intent to emphasize differences in data fusion techniques, rather than classifier architectures.

Even though feature fusion is demonstrated to enhance classification performance, it has the disadvantage of forwarding the entire extracted feature vector to a centralized unit for classification. Depending on the number of principal components or other classification features, the data load could become significant and require communication resources not necessarily affordable, especially in a long-range situational awareness scenario. As an example, a single domain and a single radar in this work already result in a feature vector

with 1120 elements. In the case of decision fusion, the classification can be performed close to each radar node in the network and would not require a substantial data transfer to a centralized processing unit. Typically, only the class prediction vector will be forwarded, with a size equal to the number of classes in the data set, e.g. 5 scalar values per sample for the demonstrated case. However, the drawback of decision fusion is the loss of degrees of freedom in combining and selecting different features in the data from different radar nodes ('feature diversity'). This, together with even lower-level fusion at signal level, could provide better classification results. Hence, an open problem remains in finding the best strategies for a given application and radar network.

REFERENCES

[1] W. W. Howard, A. F. Martone, and R. M. Buehrer, "Adversarial Multi-Player Bandits for Cognitive Radar Networks," in *2022 IEEE Radar Conference (RadarConf22)*, 2022, pp. 1–6, doi: 10.1109/RadarConf2248738.2022.9764226.

[2] U. M. Khan, Z. Kabir, S. A. Hassan, and S. H. Ahmed, "A Deep Learning Framework Using Passive WiFi Sensing for Respiration Monitoring," in *GLOBECOM 2017 - 2017 IEEE Global Communications Conference*, 2017, pp. 1–6, doi: 10.1109/GLOCOM.2017.8255027.

[3] F. Fioranelli, M. Ritchie, and H. Griffiths, "Classification of Unarmed/Armed Personnel Using the NetRAD Multistatic Radar for Micro-Doppler and Singular Value Decomposition Features," *IEEE Geosci. Remote Sens. Lett.*, vol. 12, no. 9, pp. 1933–1937, 2015.

[4] G. E. Smith, K. Woodbridge, C. J. Baker, and H. Griffiths, "Multistatic micro-Doppler radar signatures of personnel targets," *IET Signal Process.*, vol. 4, no. 3, pp. 224–233, Jun. 2010, [Online]. Available: https://digital-library.theiet.org/content/journals/10.1049/iet-spr.2009.0058.

[5] D. P. Fairchild and R. M. Narayanan, "Multistatic micro-doppler radar for determining target orientation and activity classification," *IEEE Trans. Aerosp. Electron. Syst.*, vol. 52, no. 1, pp. 512–521, 2016, doi: 10.1109/TAES.2015.130595.

[6] P. Beasley *et al.*, "Multistatic Radar Measurements of UAVs at X-band and L-band," in *2020 IEEE Radar Conference (RadarConf20)*, 2020, pp. 1–6, doi: 10.1109/RadarConf2043947.2020.9266444.

[7] D. Dhulashia, M. Temiz, and M. A. Ritchie, "Jamming Effects on Hybrid Multistatic Radar Network Range and Velocity Estimation Errors," *IEEE Access*, vol. 10, pp. 27736–27749, 2022, doi: 10.1109/ACCESS.2022.3157607.

[8] B. Fu, N. Damer, F. Kirchbuchner, and A. Kuijper, "Sensing Technology for Human Activity Recognition: A Comprehensive Survey," *IEEE Access*, vol. 8, pp. 83791–83820, 2020, doi: 10.1109/ACCESS.2020.2991891.

[9] I. Alnujaim, S. S. Ram, D. Oh, and Y. Kim, "Synthesis of Micro-Doppler Signatures of Human Activities From Different Aspect Angles Using Generative Adversarial Networks," *IEEE Access*, vol. 9, pp. 46422–46429, 2021, doi: 10.1109/ACCESS.2021.3068075.

[10] M. Pham, D. Yang, and W. Sheng, "A Sensor Fusion Approach to Indoor Human Localization Based on Environmental and Wearable Sensors," *IEEE Trans. Autom. Sci. Eng.*, vol. 16, no. 1, pp. 339–350, 2019, doi: 10.1109/TASE.2018.2874487.

[11] M. Wang, Y. D. Zhang, and G. Cui, "Human motion recognition exploiting radar with stacked recurrent neural network," *Digit. Signal Process. A Rev. J.*, vol. 87, pp. 125–131, 2019, doi: 10.1016/j.dsp.2019.01.013.

[12] C. Ding *et al.*, "Continuous Human Motion Recognition With a Dynamic Range-Doppler Trajectory Method Based on FMCW Radar," *IEEE Trans. Geosci. Remote Sens.*, vol. 57, no. 9, pp. 6821–6831, 2019, doi: 10.1109/TGRS.2019.2908758.

[13] H. Li, A. Mehul, J. Le Kernec, S. Z. Gurbuz, and F. Fioranelli, "Sequential Human Gait

Classification With Distributed Radar Sensor Fusion," *IEEE Sens. J.*, vol. 21, no. 6, pp. 7590–7603, Mar. 2021, doi: 10.1109/JSEN.2020.3046991.

[14] R. G. Guendel, M. Unterhorst, F. Fioranelli, and A. Yarovoy, "Dataset of continuous human activities performed in arbitrary directions collected with a distributed radar network of five nodes," 2021, doi: https://doi.org/10.4121/16691500.v2.

[15] A. Petroff, "A practical, high performance Ultra-Wideband radar platform," in *2012 IEEE Radar Conference*, 2012, pp. 880–884, doi: 10.1109/RADAR.2012.6212261.

[16] R. G. Guendel, F. Fioranelli, and A. Yarovoy, "Phase-Based Classification for Arm Gesture and Gross-Motor Activities Using Histogram of Oriented Gradients," *IEEE Sens. J.*, vol. 21, no. 6, pp. 7918–7927, 2021, doi: 10.1109/JSEN.2020.3044675.

[17] R. G. Guendel, F. Fioranelli, and A. Yarovoy, "Distributed radar fusion and recurrent networks for classification of continuous human activities," *IET Radar, Sonar Navig.*, doi: https://doi.org/10.1049/rsn2.12249.

[18] R. G. Guendel, M. Unterhorst, E. Gambi, F. Fioranelli, and A. Yarovoy, "Continuous human activity recognition for arbitrary directions with distributed radars," in *2021 IEEE Radar Conference (RadarConf21)*, 2021, p. 6, doi: 10.1109/RadarConf2147009.2021.9454972.

[19] F. Fioranelli, M. Ritchie, and H. Griffiths, "Aspect angle dependence and multistatic data fusion for micro-Doppler classification of armed/unarmed personnel," *IET Radar, Sonar Navig.*, vol. 9, no. 9, pp. 1231-1239(8), Dec. 2015.

[20] M. A. O. Vasilescu and D. Terzopoulos, "Multilinear subspace analysis of image ensembles," in *2003 IEEE Computer Society Conference on Computer Vision and Pattern Recognition, 2003. Proceedings.*, 2003, vol. 2, pp. II–93, doi: 10.1109/CVPR.2003.1211457.

[21] Jian Yang, D. Zhang, A. F. Frangi, and Jing-yu Yang, "Two-dimensional pca: a new approach to appearance-based face representation and recognition," *IEEE Trans. Pattern Anal. Mach. Intell.*, vol. 26, no. 1, pp. 131–137, Jan. 2004, doi: 10.1109/TPAMI.2004.1261097.

[22] J. Hua, Z. Xiong, J. Lowey, E. Suh, and E. R. Dougherty, "Optimal number of features as a function of sample size for various classification rules," *Bioinformatics*, vol. 21, no. 8, pp. 1509–1515, May 2004, doi: 10.1093/bioinformatics/bti171.

[23] G. C. Cawley and N. L. C. Talbot, "On Over-Fitting in Model Selection and Subsequent Selection Bias in Performance Evaluation," *J. Mach. Learn. Res.*, vol. 11, pp. 2079–2107, Aug. 2010.

[24] W. Troy, M. Thompson, and Y. Li, "ISAR imaging of rotating blades with an UWB radar," *2015 Texas Symp. Wirel. Microw. Circuits Syst. WMCS 2015*, pp. 13–16, 2015, doi: 10.1109/WMCaS.2015.7233213.

Author/Speaker Biographies

R. G. Guendel received his Diploma-Engineering degree (Dipl.-Ing. (FH)) from the University of Applied Sciences Zwickau in Germany. He worked at the Fraunhofer Institute for Machine Tools and Forming Technology (IWU). In 2017/18 he joined Villanova University (USA) as a Fulbright scholar in Electrical Engineering. Over summer 2018, he worked on vehicular wireless communications at the Vodafone Chair Dresden guided by Prof. Gerhard Fettweis. In 18/19, the Center for Advanced Communications of Villanova University offered him a research assistantship under Dr. Moeness G. Amin, working on continuous activity classification. He graduated with a Master of Science degree in Signal Processing and Communications in 2019. Since January 2020 he is pursuing his Ph.D. at Delft University of Technology. He works on monitoring continuous human activities in range and time beyond micro-Doppler by using RF-sensing

technology.

N. Kruse received the B.Sc. degree in Applied Physics from the Delft University of Technology in 2017 and the M.Sc degree in Theoretical Physics from the University of Groningen in 2020. He joined the Microwave Sensing, Systems, and Signals group at the Delft University of Technology in March of 2021, where he is currently researching the classification of continuous human activities.

F. Fioranelli received his Laurea (BEng, cum laude) and Laurea Specialistica (MEng, cum laude) degrees in telecommunication engineering from the Università Politecnica delle Marche, Ancona, Italy, in 2007 and 2010, respectively, and the Ph.D. degree from Durham University, U.K., in 2014. He is currently an Assistant Professor at TU Delft in the Netherlands, and was an Assistant Professor at the University of Glasgow (2016-2019) and Research Associate at University College London (2014-2016).
His research interests include the development of radar systems and automatic classification for human signatures analysis in healthcare and security, UAVs detection and classification, automotive radar, wind farm and sea clutter. He has authored over 120 publications between book chapters, journal and conference papers, edited the books on “Micro-Doppler Radar and Its Applications” and “Radar Countermeasures for Unmanned Aerial Vehicles” published by IET-Scitech, and received three best paper awards.

Olexander Yarovyi (Engl.: Alexander Yarovoy) graduated from the Kharkov State University, Ukraine, in 1984 with the Diploma with honor in radiophysics and electronics. He received the Candidate Phys. & Math. Sci. and Doctor Phys. & Math. Sci. degrees in radiophysics in 1987 and 1994, respectively.
In 1987 he joined the Department of Radiophysics at the Kharkov State University as a Researcher and became a Full Professor there in 1997. From September 1994 through 1996 he was with Technical University of Ilmenau, Germany as a Visiting Researcher. Since 1999 he is with the Delft University of Technology, the Netherlands. Since 2009 he leads there a chair of Microwave Sensing, Systems and Signals. His main research interests are in high-resolution radar, microwave imaging and applied electromagnetics (in particular, UWB antennas). He has authored and co-authored more than 450 scientific or technical papers, six patents and fourteen book chapters. He is the recipient of the European Microwave Week Radar Award for the paper that best advances the state-of-the-art in radar technology in 2001 (together with L.P. Ligthart and P. van Genderen) and in 2012 (together with T. Savelyev). In 2010 together with D. Caratelli Prof. Yarovoy got the best paper award of the Applied Computational Electromagnetic Society (ACES).
Prof. Yarovoy served as the Chair and TPC chair of the 5th European Radar Conference (EuRA'08), Amsterdam, the Netherlands, as well as the Secretary of the 1st European Radar Conference (EuRAD'04), Amsterdam, the Netherlands. He served also as the co-chair and TPC chair of the Xth International Conference on GPR (GPR2004) in Delft, the Netherlands. He served as an Associated Editor of the International Journal of Microwave and Wireless Technologies from 2011 till 2018 and as a Guest Editor of five special issues of the IEEE Transactions and other journals. In the period 2008-2017 Prof. Yarovoy served as Director of the European Microwave Association (EuMA).